

Conduction mechanisms, molecular modelling and micro-Raman studies of TlInSe₂ chalcogenide crystal

NEVIN KALKAN^a*, SEFA CELIK^b, HANIFE BAS^c, AYSEN E. OZEL^a

^a*Istanbul University, Science Faculty, Physics Department, 34134, Istanbul, Turkey*

^b*Istanbul University, Engineering Faculty, Electrical and Electronics Engineering Department, 34320, Istanbul, Turkey*

^c*Yildiz Technical University, Faculty of Arts and Science, Physics Department, 34349, Istanbul, Turkey*

The temperature dependence of the electrical conductivity of the sample was studied for temperatures between 120 and 330 Kelvin. The DC measurements suggest that the electrical transport is governed by space charge limited conduction mechanism in the temperature range (210-330 K) and the related parameters, such as trap density, activation energy were calculated. The ac conductivity of the studied sample was investigated in the frequency range 10 Hz-20MHz and temperature range 173-373 K. The temperature dependence of both the ac conductivity and the frequency exponent, s is reasonably well interpreted in terms of the correlated barrier hopping model. Molecular Mechanics calculations with universal force field were performed on the TlIn₄Se₁₆ cluster that represent the local structure of the investigated crystal. The optimal geometries and the vibrational properties of the investigated cluster were calculated using universal force field method.

(Received May 17, 2016; accepted April 6, 2017)

Keywords: Space charge limited conduction, ternary crystals, TlInSe₂, micro-Raman spectroscopy, correlated barrier hopping

1. Introduction

The compound TlInSe₂ belongs to the group of ternary semiconductors of the A^{III}B^{III}C^{VI}₂ type. The TlInSe₂ compound, as a tetragonal lattice having parameters $a=8.075$ Å and $c=6.847$ Å with a group symmetry $D_{4h}^{18}-I4/mcm$, is one of the partial valence ternary layer-chain semiconductors [1]. Ternary semiconductive compounds TlInSe₂ have interesting optical and electrical properties that make them good materials for optoelectronic device applications [1-4] and therefore they have attracted a lot of attention. The electrical, optical and electro-thermal properties of the TlInSe₂ compound have been studied previously [5-18]. Furthermore, TlInSe₂-AgInSe₂ systems, TlGaSe₂-TlInSe₂ mixed crystals, TlInSeS, TlIn(S_{1-x}Se_x)₂ and Tl_{1-x}In_{1-x}Si_xSe₂ compounds have been the subject of several studies because of their interesting features [19-23]. A study of the DC and AC conductivity mechanism of TlInSe₂ crystals by Ebnalwaled et al. found that while the Mott's variable range hopping mechanism is dominant in the low temperature region (184-211 K), termionic emission mechanism are dominant in the high temperature (369-455 K) region. The characterizations of Ag/TlInSe₂/Ag structure have been investigated by F. Qasrawi et al. in a separate study and they obtained the trapping level, trap density of space charge limited current (SCLC) mechanism at room temperature. In the same study they observed an SCLC region for In/TlInSe₂/In, however the parameters, such as trap density, were not calculated. In our previous studies, [24, 27] we investigated the electrical properties as well as the conductivity mechanism before switching to TlSbSe₂ and

TlBiSe₂. For both samples we observed the non-linear I-V characteristics. In this work we focus on TlInSe₂ ternary compound which has the similar interesting properties like TlSbSe₂ and TlBiSe₂ compounds. The aim of this work is to elucidate the dc and ac conductivity of In/TlInSe₂/In structures. The resultant actual behaviors of the dc conductivity for these samples is discussed and analyzed. Important physical parameters such as trap density, activation energy are estimated. Measurement of ac conductivity of chalcogenide semiconductors has been extensively used to understand the conduction process in these materials. In the present work, we were therefore investigated the ac conductivity in order to elucidate the mechanism responsible for the conductivity of this compound.

The novelty of this work is the determination of the temperature dependence of trap density for SCLC conductivity mechanism at 210-330 K temperature ranges. Furthermore, the frequency and temperature dependence of the ac conductivity were studied in the high frequency region (100 kHz-20MHz). Also for the first time, it was fulfilled the investigation of the optimized geometrical parameters and the assignment of the vibrational spectra which was performed based on the potential energy distribution of the vibrational modes

The first part of this paper provides an idealized molecular model (octagon) of TlInSe₂ crystal formed using Molecular Mechanics (MM) with universal force field (UFF) to calculate the optimized geometry and the vibrational wavenumbers of TlIn₄Se₁₆ cluster. In Models of the crystal structure of TlInSe₂ were presented previously by Muller [29], Gasanly [30, 31] and Kilday [11]. The molecular model of TlInSe₂ crystal and ab initio

calculations of its energy levels were calculated by Grigas based on the Hartree-Fock matrix equation's solution using the Gamess program [17].

In the second part of this study, we focus on the electrical conductivity of TlInSe₂ ternary crystals in the temperature range from 120 to 330 K. Our studies reveal that the space charge limited current conduction mechanism is predominant in these samples. Space charge is important in photoelectric cells, thermionic tubes, and particle accelerators owing to its effect on the flow of current, it also plays a part in electrical conduction in solids. Space charge limited current in insulators and semiconductors is of interest because of its technological potentials [28]. The ac conductivity of studied sample was investigated in the frequency range 10 Hz-20MHz and temperature range 173-373 K. The conductivity as a function of frequency exhibited two components: dc conductivity σ_{dc} , and ac conductivity σ_{ac} , where $\sigma_{ac} \sim \omega^s$. Here the s parameter decreases with increasing temperature. This behavior of s can comply with Correlated Barrier Hopping (CBH) model. Furthermore, the maximum barrier height W_m and activation energy E were calculated.

2. Experimental

The TlInSe₂ sample used for the measurement, was grown by direct fusion of their constituent elements, explicitly described elsewhere [9]. Micro Raman spectra (10 to 250 cm⁻¹) of the TlInSe₂ were recorded by a Jasco NRS 3100 micro Raman spectrometer (1200 lines/mm grating and high sensitivity cooled CCD) equipped with a 785 nm diode laser. Rayleigh scattering was rejected by a notch filter. The spectrometer was calibrated with the silicon phonon mode at 520 cm⁻¹. The exposure time, the accumulation, and spectral resolution were 1s, 130 spectra and 1.48 cm⁻¹, respectively. Band fitting procedures were performed using the GRAMS/AI 7.02 (Thermo Electron Corporation) software package with the Voigt function (for Raman spectrum). Converged results were obtained with squared correlations better than $r^2 \sim 0.9994$. The second derivatives of the spectra were obtained by using Savitzky-Golay function (two polynomial degrees, 13 points) which gives information about the position of the bands and band widths.

The typical dimensions of our rectangular shaped samples were $4 \times 1 \times 0.3 \text{ mm}^3$. The base and counter Au electrodes, each 3000Å thick, were deposited onto the sample in a 10^{-5} Torr vacuum. Copper wires fixed by indium on Au electrodes were used as the electrical contacts which proved to form Ohmic contacts of low resistivity with these materials. A current flow along the c -axis of the sample was ensured by a pair of contacts deposited on the two opposite surfaces of the sample. The electrical measurements were carried out in the temperature range of 10-350 K using closed cycle Helium cryostat (ARS-DE202-SE). A constant-voltage source was generated by the Keithley 2400 source meter. Furthermore, a Lake-Shore 331 temperature controller was

used to measure to control the temperature.

The typical dimensions of our rectangular shaped sample were 1.75x1.75x0.5 mm for ac measurements. The capacitance and dissipation factor of the samples were measured using a Hewlett Packard impedance analyzer (4192A) in the frequency range 10Hz-20MHz and temperature range from 173K to 373 K. Temperatures of the sample were measured with a copper-constant thermocouple. All measurements were made in approximately 10^{-4} Torr vacuum.

3. Results and discussion

3.1. Molecular Modeling Study

Geometry optimization and vibrational frequencies of TlIn₄Se₁₆ cluster as an idealized molecular model (octagon) of TlInSe₂ crystal were studied by means of the molecular mechanics methods using the UFF in Gaussian 03 [32]. The potential energy distributions (PED) of vibrational modes were computed and the force fields in Cartesian coordinates were converted to natural internal coordinates using by MOLVIB program [33, 34]. The Optimized geometry of the TlIn₄Se₁₆ cluster is modelled based on the structure given by Grigas (Fig. 1) and the parameters are tabulated in Table 1. Previous studies of the In-Se bond length in similar structure found it to be in the region 2.535-2.694 Å [35], in this work the bond length is found to be the region of 2.5008- 2.5891 Å. The Tl-Se bond length was found to be between 2.5957-2.65439 Å, a range which mostly agrees with Ref [36].

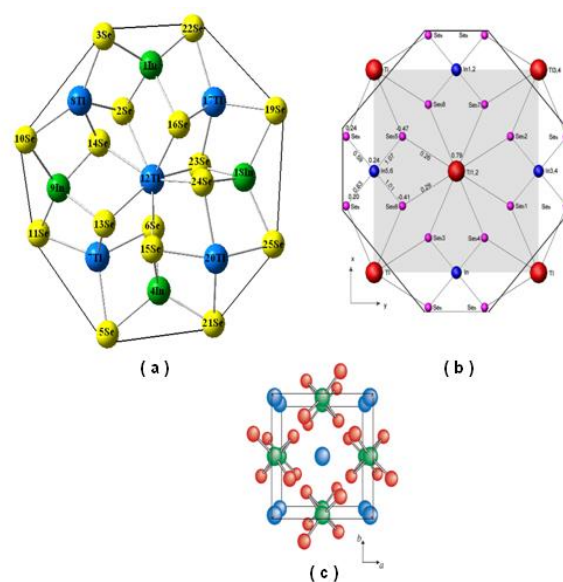


Fig.1. The structure of TlIn₄Se₁₆ cluster was obtained in our study by using Molecular Mechanics (MM) with universal force field (UFF) (a), Molecular Modeling study of TlIn₄Se₁₆ cluster carried out by J. Grigas (b) and Crystal structure of TlInSe₂ determined by Muller (c)

Table 1. Structural Parameters for $TlIn_4Se_{16}$ cluster

Atoms	$TlIn_4Se_{16}$	Atoms	$TlIn_4Se_{16}$	Atoms	$TlIn_4Se_{16}$
R(2,1)	2.5009	A(3,1,2)	103.79	A(16,12,14)	106.43
R(3,1)	2.5891	A(3,8,2)	100.07	A(17,16,1)	72.15
R(5,4)	2.5783	A(6,4,5)	107.62	A(21,4,5)	120.09
R(6,4)	2.5555	A(7,5,4)	65.51	A(21,4,6)	122.70
R(7,5)	2.6046	A(8,2,1)	76.58	A(21,4,15)	99.69
R(8,2)	2.5957	A(10,8,3)	127.50	A(22,1,2)	102.94
R(8,3)	2.6307	A(11,7,5)	117.17	A(22,1,3)	129.83
R(10,8)	2.6310	A(11,9,10)	129.82	A(22,17,19)	117.19
R(10,9)	2.5887	A(12,6,4)	91.32	A(23,12,2)	87.16
R(11,9)	2.5766	A(13,7,6)	94.82	A(23,12,13)	153.79
R(12,6)	2.7045	A(13,9,11)	108.15	A(23,12,14)	103.03
R(13,9)	2.5124	A(14,9,13)	89.85	A(23,12,15)	119.56
R(14,9)	2.5008	A(14,12,2)	30.72	A(23,12,16)	91.94
R(15,4)	2.5425	A(14,12,13)	80.97	A(23,18,19)	107.61
R(16,1)	2.5123	A(15,4,5)	109.11	A(24,12,14)	152.40
R(17,16)	2.6466	A(15,4,6)	92.35	A(24,12,15)	67.46
R(19,18)	2.5784	A(15,12,2)	152.39	A(24,12,16)	46.37
R(20,15)	2.6302	A(15,12,6)	85.01	A(24,12,23)	85.07
R(21,4)	2.5359	A(15,12,13)	46.45	A(25,18,19)	120.20
R(22,1)	2.5767	A(15,12,14)	126.34	A(25,18,23)	122.54
R(23,18)	2.5549	A(16,1,2)	89.85	A(25,18,24)	99.75
R(25,18)	2.5354	A(16,12,2)	80.97	A(25,20,21)	86.43

The MM/UFF computational and PED results (Table 2) give wavenumbers of the Se-In stretching modes of $TlIn_4Se_{16}$ cluster at 277 cm^{-1} with a PED of 18%, 276 cm^{-1} with a PED of 20%, 271 cm^{-1} with a PED of 22%, 269 cm^{-1} with a PED of 25%, 262 cm^{-1} with a PED of 25%, 257 cm^{-1} with a PED of 30% and 236 cm^{-1} with a

PED of 15% and the wavenumbers of Tl-Se stretching modes at 255 cm^{-1} with a PED of 14% and 243 cm^{-1} with a PED of 30% and 8%. In the Raman study of Ref [37] the In-Se stretching mode is assigned a value of 213 cm^{-1} as a weak band.

Table 2. Calculated wavenumbers (cm^{-1}) and the potential energy distribution of the vibrational modes of the $TlIn_4Se_{16}$ cluster

Assignment	MM/UFF	PED%	
		$TlIn_4Se_{16}$ cluster form	MM/UFF
	ν_{cal}		
δ_{TlSeIn}	299	$\delta_{TlSeIn}(28)+\delta_{InSeIn}(9)+\Gamma_{SeInSeSe}(8)+\nu_{SeIn}(8)$	
$\Gamma_{SeInSeSe}$	288	$\Gamma_{SeInSeSe}(24)+\Gamma_{SeInSeIn}(8)+\delta_{SeInTi}(6)+\delta_{TlSeIn}(6)$	
δ_{TlSeIn}	286	$\delta_{TlSeIn}(18)+\nu_{SeIn}(12)+\Gamma_{SeSeInSe}(8)+\Gamma_{SeTlSeIn}(7)+\delta_{SeInSe}(6)$	
δ_{TlSeIn}	284	$\delta_{TlSeIn}(25)+\nu_{SeIn}(15)+\delta_{SeInSe}(15)+\Gamma_{SeSeInSe}(7)$	
$\Gamma_{SeInSeSe}$	282	$\Gamma_{SeInSeSe}(41)+\delta_{SeInTi}(6)+\Gamma_{SeInSeIn}(6)$	
δ_{SeInSe}	281	$\delta_{SeInSe}(23)+\nu_{SeIn}(16)+\delta_{TlSeIn}(13)$	
$\Gamma_{SeInSeIn}$	281	$\Gamma_{SeInSeIn}(13)+\Gamma_{InTlSeIn}(12)+\nu_{SeIn}(11)$	
ν_{SeIn}	277	$\nu_{SeIn}(18)+\Gamma_{InTlSeIn}(10)+\Gamma_{TlSeInSe}(9)+\Gamma_{SeInTlSe}(8)+\delta_{TlSeIn}(8)$	
ν_{SeIn}	276	$\nu_{SeIn}(20)+\delta_{TlSeIn}(14)+\Gamma_{SeInTlSe}(9)+\Gamma_{SeInSeIn}(8)+\Gamma_{InTlSeIn}(7)+\Gamma_{TlSeInSe}(5)$	
ν_{SeIn}	271	$\nu_{SeIn}(22)+\delta_{TlSeIn}(11)+\Gamma_{SeSeInSe}(8)+\Gamma_{SeInTlSe}(5)$	
ν_{SeIn}	269	$\nu_{SeIn}(25)+\delta_{TlSeIn}(12)+\Gamma_{InTlSeIn}(6)$	
ν_{SeIn}	262	$\nu_{SeIn}(25)+\delta_{TlSeIn}(9)+\nu_{TlSe}(8)+\delta_{SeInSe}(6)$	
δ_{SeInSe}	259	$\delta_{SeInSe}(27)+\delta_{TlSeIn}(25)$	
ν_{SeIn}	257	$\nu_{SeIn}(30)+\Gamma_{TlSeIn}(6)+\Gamma_{InSeIn}(5)$	
ν_{TlSe}	255	$\nu_{TlSe}(14)+\delta_{InTlSe}(8)+\nu_{SeIn}(7)+\delta_{InSeIn}(7)+\Gamma_{TlSeInSe}(6)+\delta_{SeInSe}(5)$	
ν_{TlSe}	243	$\nu_{TlSe}(30)+\delta_{SeTlSe}(9)+\nu_{SeSe}(6)+\delta_{SeSeIn}(6)$	
ν_{TlSe}	243	$\nu_{TlSe}(8)+\delta_{TlInTi}(7)+\Gamma_{SeSeInSe}(6)+\nu_{SeSe}(6)+\delta_{InTlSe}(6)+\nu_{SeIn}(6)$	

Assignment	MM/UFF	PED%	
		TlInSe ₂ cluster form	MM/UFF
Γ_{SeInSeIn}	242	$\Gamma_{\text{SeInSeIn}}(14) + \delta_{\text{SeInSe}}(11) + \nu_{\text{TlSe}}(11) + \Gamma_{\text{SeTlSeIn}}(6) + \delta_{\text{TlSeIn}}(6) + \delta_{\text{SeSeIn}}(5)$	
Γ_{SeInSeSe}	240	$\Gamma_{\text{SeInSeSe}}(67) + \delta_{\text{SeSeIn}}(6) + \Gamma_{\text{SeInSeIn}}(6)$	
δ_{SeInSe}	238	$\delta_{\text{SeInSe}}(20) + \Gamma_{\text{SeInSeIn}}(9) + \Gamma_{\text{InTlSeIn}}(7)$	
ν_{SeIn}	236	$\nu_{\text{SeIn}}(15) + \Gamma_{\text{SeInSeIn}}(13) + \delta_{\text{SeInSe}}(10) + \nu_{\text{SeSe}}(9) + \nu_{\text{TlSe}}(8) + \Gamma_{\text{SeInTlSe}}(6)$	
δ_{TlSeIn}	226	$\delta_{\text{TlSeIn}}(24) + \delta_{\text{SeInTl}}(11) + \delta_{\text{SeInSe}}(7) + \Gamma_{\text{SeInSeSe}}(7)$	
Γ_{SeInSeSe}	225	$\Gamma_{\text{SeInSeSe}}(37) + \delta_{\text{SeInTl}}(14)$	
Γ_{InTlSeIn}	220	$\Gamma_{\text{InTlSeIn}}(15) + \Gamma_{\text{SeInTlSe}}(13) + \delta_{\text{TlSeIn}}(10) + \delta_{\text{SeInTl}}(8) + \Gamma_{\text{SeInSeSe}}(5)$	
Γ_{InTlSeIn}	215	$\Gamma_{\text{InTlSeIn}}(25) + \Gamma_{\text{SeInTlSe}}(17) + \delta_{\text{SeInTl}}(8) + \delta_{\text{TlSeIn}}(5)$	
Γ_{InTlSeIn}	212	$\Gamma_{\text{InTlSeIn}}(16) + \Gamma_{\text{SeInTlSe}}(15) + \delta_{\text{SeInSe}}(6)$	
δ_{SeInSe}	211	$\delta_{\text{SeInSe}}(17) + \delta_{\text{TlSeIn}}(16) + \nu_{\text{TlSe}}(12) + \nu_{\text{SeIn}}(6)$	
δ_{TlSeIn}	206	$\delta_{\text{TlSeIn}}(15) + \delta_{\text{SeInSe}}(13) + \nu_{\text{TlSe}}(12)$	
Γ_{InTlSeIn}	205	$\Gamma_{\text{InTlSeIn}}(22) + \Gamma_{\text{SeInTlSe}}(14) + \delta_{\text{SeInTl}}(9) + \delta_{\text{InSeIn}}(6)$	
Γ_{SeSeInSe}	201	$\Gamma_{\text{SeSeInSe}}(58) + \Gamma_{\text{SeInTlSe}}(8) + \Gamma_{\text{InTlSeIn}}(7)$	
δ_{TlSeIn}	200	$\delta_{\text{TlSeIn}}(14) + \Gamma_{\text{SeInSeIn}}(12) + \Gamma_{\text{SeInTlSe}}(11) + \delta_{\text{SeInSe}}(16)$	
δ_{SeInSe}	194	$\delta_{\text{SeInSe}}(22) + \nu_{\text{TlSe}}(16) + \delta_{\text{TlSeIn}}(11) + \delta_{\text{SeSeIn}}(11) + \Gamma_{\text{InTlSeIn}}(8)$	
Γ_{SeInSeSe}	192	$\Gamma_{\text{SeInSeSe}}(91)$	
Γ_{SeInSeIn}	191	$\Gamma_{\text{SeInSeIn}}(16) + \Gamma_{\text{InTlSeIn}}(12) + \Gamma_{\text{SeSeInTl}}(8) + \delta_{\text{InTlSe}}(8) + \delta_{\text{SeSeIn}}(7)$	
Γ_{SeInSeSe}	186	$\Gamma_{\text{SeInSeSe}}(24) + \Gamma_{\text{SeInSeIn}}(23) + \Gamma_{\text{TlSeInSe}}(7) + \delta_{\text{TlSeIn}}(6) + \nu_{\text{TlSe}}(6)$	
Γ_{SeInSeSe}	186	$\Gamma_{\text{SeInSeSe}}(14) + \Gamma_{\text{SeInSeIn}}(13) + \Gamma_{\text{InTlSeIn}}(7) + \delta_{\text{InSeIn}}(6)$	
δ_{SeInSe}	184	$\delta_{\text{SeInSe}}(19) + \Gamma_{\text{SeSeInTl}}(15) + \delta_{\text{TlSeIn}}(8) + \delta_{\text{SeInTl}}(7)$	
Γ_{SeInSeSe}	177	$\Gamma_{\text{SeInSeSe}}(87)$	
Γ_{SeInSeIn}	173	$\Gamma_{\text{SeInSeIn}}(24) + \delta_{\text{SeInSe}}(10) + \delta_{\text{TlSeIn}}(7) + \Gamma_{\text{InTlSeIn}}(7) + \delta_{\text{InTlSe}}(6) + \Gamma_{\text{TlSeInSe}}(6)$	
δ_{SeInSe}	172	$\delta_{\text{SeInSe}}(31) + \Gamma_{\text{InTlSeIn}}(9)$	
Γ_{SeInSeSe}	139	$\Gamma_{\text{SeInSeSe}}(23) + \delta_{\text{InSeIn}}(12) + \delta_{\text{TlSeIn}}(12) + \delta_{\text{SeInSe}}(18)$	
Γ_{SeInSeSe}	133	$\Gamma_{\text{SeInSeSe}}(31) + \delta_{\text{SeInSe}}(13) + \delta_{\text{TlSeIn}}(10) + \Gamma_{\text{SeInTlSe}}(8) + \Gamma_{\text{TlSeInSe}}(8)$	
Γ_{SeInSeSe}	116	$\Gamma_{\text{SeInSeSe}}(20) + \delta_{\text{TlSeIn}}(12) + \delta_{\text{SeInSe}}(9) + \delta_{\text{InSeIn}}(7) + \Gamma_{\text{SeInSeIn}}(6)$	
δ_{TlSeIn}	112	$\delta_{\text{TlSeIn}}(39) + \delta_{\text{SeInSe}}(17) + \nu_{\text{InTl}}(8) + \Gamma_{\text{SeInSeIn}}(6)$	
Γ_{InTlSeIn}	110	$\Gamma_{\text{InTlSeIn}}(33) + \Gamma_{\text{SeInTlSe}}(26)$	
Γ_{InTlSeIn}	103	$\Gamma_{\text{InTlSeIn}}(40) + \Gamma_{\text{SeInTlSe}}(27)$	
δ_{TlSeIn}	101	$\delta_{\text{TlSeIn}}(25) + \Gamma_{\text{SeInTlSe}}(17) + \delta_{\text{SeInSe}}(12) + \Gamma_{\text{SeTlInTl}}(8) + \Gamma_{\text{TlSeInSe}}(7) + \delta_{\text{TlInTl}}(6)$	
δ_{InTlSe}	97	$\delta_{\text{InTlSe}}(14) + \delta_{\text{SeInSe}}(11) + \Gamma_{\text{SeInSeIn}}(9) + \delta_{\text{TlSeIn}}(7) + \Gamma_{\text{TlSeInSe}}(5) + \nu_{\text{InSe}}(5)$	
Γ_{SeInSeIn}	96	$\Gamma_{\text{SeInSeIn}}(22) + \Gamma_{\text{InTlSeIn}}(16) + \delta_{\text{TlSeIn}}(8) + \Gamma_{\text{TlSeInSe}}(7) + \delta_{\text{InTlSe}}(6)$	
δ_{TlSeIn}	95	$\delta_{\text{TlSeIn}}(22) + \delta_{\text{SeInSe}}(18) + \Gamma_{\text{InTlSeIn}}(12) + \delta_{\text{InTlSe}}(6)$	
Γ_{InTlSeIn}	91	$\Gamma_{\text{InTlSeIn}}(28) + \Gamma_{\text{SeInSeSe}}(11) + \delta_{\text{InTlSe}}(11) + \Gamma_{\text{SeInTlSe}}(7)$	
δ_{InTlSe}	85	$\delta_{\text{InTlSe}}(29) + \Gamma_{\text{TlSeInSe}}(12) + \nu_{\text{SeSe}}(10) + \delta_{\text{TlSeIn}}(6)$	
Γ_{TlSeInSe}	85	$\Gamma_{\text{TlSeInSe}}(33) + \delta_{\text{InTlSe}}(33) + \Gamma_{\text{SeInSeIn}}(12) + \Gamma_{\text{SeInTlSe}}(10)$	
Γ_{InTlSeIn}	82	$\Gamma_{\text{InTlSeIn}}(23) + \Gamma_{\text{SeInSeIn}}(10) + \delta_{\text{InSeIn}}(7) + \delta_{\text{InTlSe}}(6) + \delta_{\text{SeInSe}}(6)$	
Γ_{SeInSeIn}	81	$\Gamma_{\text{SeInSeIn}}(22) + \Gamma_{\text{SeSeInSe}}(20) + \delta_{\text{InTlSe}}(18) + \Gamma_{\text{TlSeInSe}}(13)$	
δ_{InTlSe}	77	$\delta_{\text{InTlSe}}(28) + \Gamma_{\text{TlSeInSe}}(9) + \Gamma_{\text{SeInTlSe}}(8) + \Gamma_{\text{InTlSeIn}}(7)$	
Γ_{InSeInSe}	73	$\Gamma_{\text{InSeInSe}}(22) + \Gamma_{\text{SeSeInSe}}(10) + \nu_{\text{InSe}}(8) + \nu_{\text{InTl}}(5)$	
δ_{SeInSe}	69	$\delta_{\text{SeInSe}}(25) + \delta_{\text{InTlSe}}(22) + \delta_{\text{TlSeIn}}(16) + \Gamma_{\text{TlSeInSe}}(6)$	
δ_{InTlSe}	68	$\delta_{\text{InTlSe}}(16) + \Gamma_{\text{SeInSeIn}}(14) + \Gamma_{\text{InTlSeIn}}(8) + \delta_{\text{TlSeIn}}(8) + \Gamma_{\text{SeInTlSe}}(6)$	
δ_{TlSeIn}	66	$\delta_{\text{TlSeIn}}(15) + \delta_{\text{TlInTl}}(12) + \Gamma_{\text{TlSeInSe}}(12) + \Gamma_{\text{InTlSeIn}}(12) + \delta_{\text{SeInSe}}(12) + \Gamma_{\text{SeInTlSe}}(8)$	
Γ_{TlSeInSe}	63	$\Gamma_{\text{TlSeInSe}}(20) + \Gamma_{\text{SeInSeIn}}(12) + \delta_{\text{SeInSe}}(8) + \Gamma_{\text{SeInSeSe}}(7) + \delta_{\text{TlSeIn}}(7)$	
Γ_{InSeInSe}	59	$\Gamma_{\text{InSeInSe}}(20) + \Gamma_{\text{SeInTlSe}}(16) + \Gamma_{\text{InTlSeIn}}(10) + \Gamma_{\text{TlSeInSe}}(6)$	
δ_{TlSeIn}	56	$\delta_{\text{TlSeIn}}(18) + \Gamma_{\text{SeInSeSe}}(8) + \delta_{\text{InTlSe}}(7)$	
δ_{SeInSe}	52	$\delta_{\text{SeInSe}}(18) + \Gamma_{\text{InSeInSe}}(17) + \delta_{\text{InTlSe}}(14) + \Gamma_{\text{TlSeInSe}}(9) + \Gamma_{\text{InTlSeIn}}(8)$	
Γ_{InSeInSe}	43	$\Gamma_{\text{InSeInSe}}(34) + \delta_{\text{InTlSe}}(14) + \delta_{\text{SeInSe}}(9) + \Gamma_{\text{InTlSeIn}}(6)$	
Γ_{InTlSeIn}	33	$\Gamma_{\text{InTlSeIn}}(18) + \delta_{\text{InSeIn}}(15) + \Gamma_{\text{InSeInSe}}(15) + \Gamma_{\text{TlSeInSe}}(8)$	
Γ_{SeInSeIn}	31	$\Gamma_{\text{SeInSeIn}}(38) + \delta_{\text{SeInSe}}(9) + \Gamma_{\text{InTlSeIn}}(6) + \delta_{\text{InTlSe}}(6)$	
Γ_{SeInSeIn}	19	$\Gamma_{\text{SeInSeIn}}(53) + \Gamma_{\text{InTlSeIn}}(9) + \delta_{\text{InTlSe}}(7)$	
δ_{InTlSe}	15	$\delta_{\text{InTlSe}}(20) + \Gamma_{\text{InTlSeIn}}(16) + \Gamma_{\text{InSeInSe}}(8) + \Gamma_{\text{TlSeInSe}}(8) + \delta_{\text{SeTlSe}}(6)$	

3.2. Raman Study

The characteristic vibrational frequencies of TlInSe₂ crystal were observed using Micro Raman spectrometer. The observed frequencies are in agreement with previously reported Raman results for TlInSe₂ [30, 31, 38, 39] and are given in Table 3 and Fig. 2. TlInSe₂ shows characteristic bands at 210, 199, 193, 183, 172, 111, 96, 59, 49, 32, 17 cm⁻¹, and at 166, 153 cm⁻¹, assigned to combination bands (111+59 cm⁻¹, 111+49 cm⁻¹) in Raman spectrum. The band component analysis of the 205- 145 cm⁻¹ region of the Raman spectrum of TlInSe₂, in comparison with the second derivative profile is given in Fig. 2. The bands at 199, 193, 183, 172, 166 and 153 cm⁻¹ are inferred from both the second derivative and band component analysis.

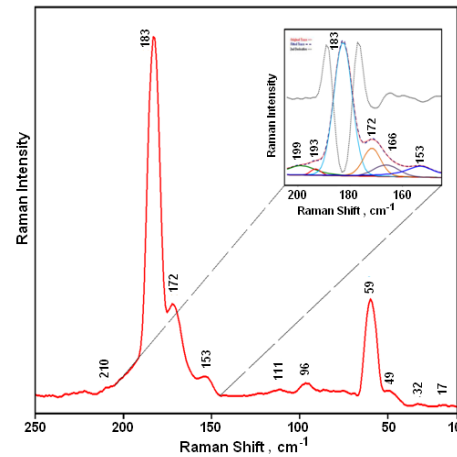


Fig. 2. The Experimental Raman spectrum of TlInSe₂

Table 3. The vibrational frequencies of the TlInSe₂ crystal in comparison with literature results

TlInSe ₂	[30]	[31]	[38]	[39]
Raman	Raman	Raman	Raman	Raman
210		212 (E _u)	210 (E _u)	212 (E _u)
199	200 (B _{1g})	200 (B _{2g})	200 (B _{1g})	200 (B _{2g})
193		196 (E _u)	193(E _u)	196 (E _u)
183	184 (A _{1g})	179 (A _{2u})	184 (A _{1g})	184 (A _{1g})
172	174 (E _g)		174 (E _g)	174 (E _g)
111		114 (E _u)	114 (E _u)	114 (E _u)
96	98 (B _{2g})	98 (E _u)	98 (B _g)	98(B _{1g})
59	60 (E _g)	61 (E _u)	60(E _g)	60 (E _g)
49		54 (E _u)	48(E _u)	54 (E _u)
32	30 (E _g)	28 (A _{2u})	30 (E _g)	30 (E _g)
17	16 (B _{2g})			

3.3. DC Conductivity

The current-voltage (I-V) characteristics of the sample was measured in the temperature range 120-330 K. The plot of resistivity (ρ) versus temperature (T) of TlInSe₂ ternary compound is shown in Fig. 3.

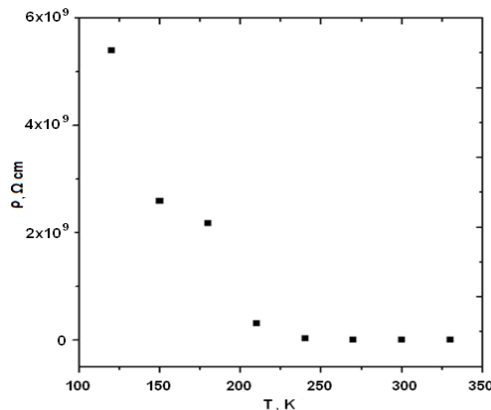


Fig. 3. Temperature dependence of the resistivity of TlInSe₂ ternary compound

In the ohmic region of each I-V characteristic, the conductivity σ_{dc} was estimated. The corresponding $\ln \sigma_{dc}$ versus $10^3/T$ curve is given in Fig. 4. It was observed that, in the temperature range 120-330K, the electrical conductivity increases with increasing temperature for these samples, as is typical for semiconductors, in accordance with the thermionic emission relation

$$\sigma = \sigma_0 \exp\left(\frac{-\Delta E_\sigma}{k_B T}\right) \quad (1)$$

where σ_0 is the pre-exponential factor, k_B is the Boltzmann constant, T is the absolute temperature and ΔE_σ is the conduction activation energy. The value of ΔE_σ is calculated from the slope of the line of Fig. 4 according to Eq. (1).

The obtained value of ΔE_σ was found to be 0.34 eV. With increasing temperature, more charge carriers overcome the activation energy barrier and these carriers participate in the electrical conduction. This indicates that the conduction in this sample is due to an activated process. Fig. 5 shows the logI-logV curves of TlInSe₂ sample for different temperatures.

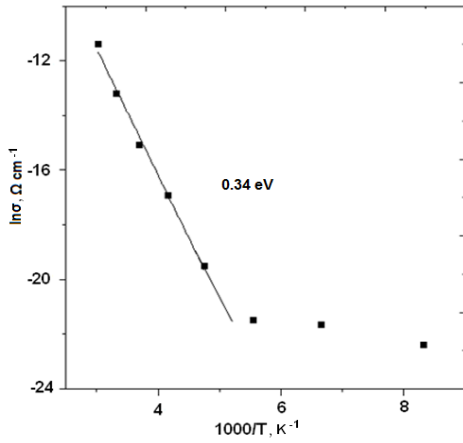


Fig. 4. Temperature dependence of the conductivity of TlInSe₂ ternary compound

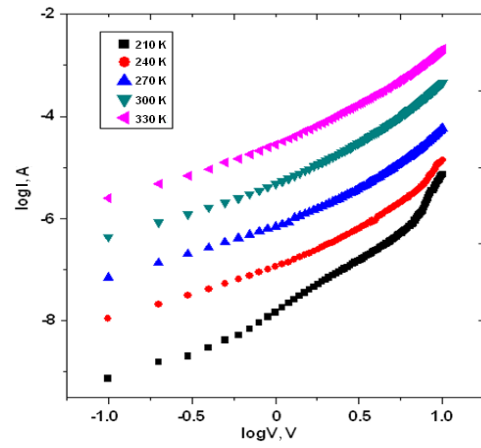
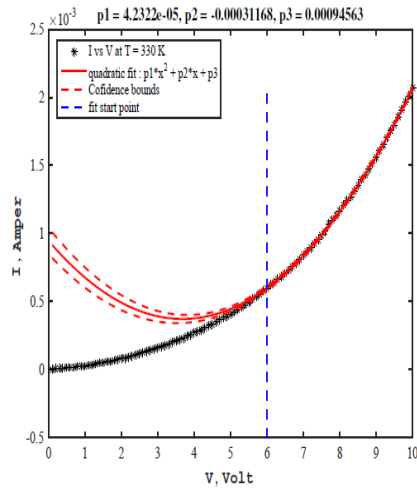
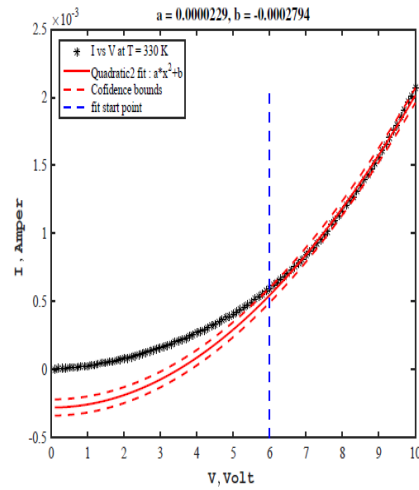


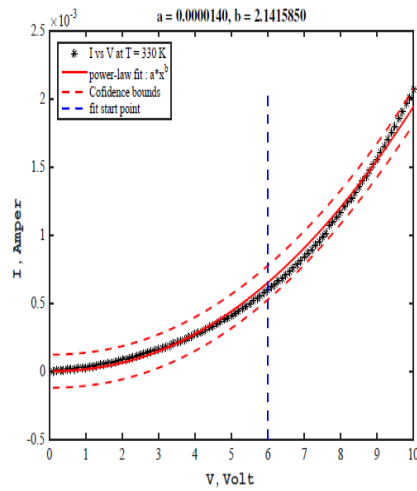
Fig. 5. logI-logV characteristics at different temperatures



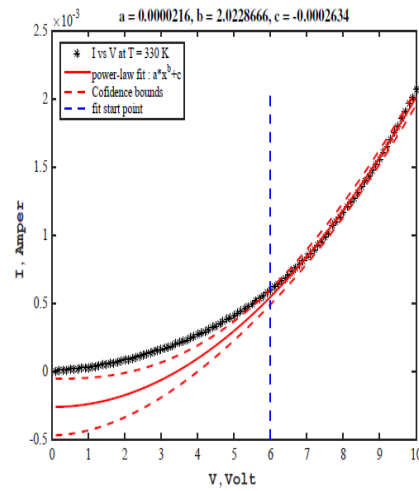
(a)



(b)



(c)



(d)

Fig. 6. Current (I) versus Voltage (V) data with various fits for a range of temperatures

Table 4. Various $I - V$ fit functions and their fit parameters and properties

Fit	T (K)	sse	r-square	adj-rsquare	rmse	dfe	Fit parameters
Quadratic-1 $f(x) = p_1 x^2 + p_2 x + p_3$	330	1.3857×10^{-9}	0.9998	0.9998	6.0387×10^{-6}	38	$p_1 p_2 = 4.232 \times 10^{-5}$ $p_3 = -0.0003117$ $= 0.0009456 \times 10^{-5}$
Quadratic-2 $f(x) = p_1 x^2 + p_2$	330	2.5632×10^{-8}	0.9967	0.9966	2.5637×10^{-5}	39	$p_1 p_2 = 2.293 \times 10^{-5}$ $= -0.0002794$
Power-1 $f(x) = a x^b$	330	2.7411×10^{-7}	0.9920	0.9920	5.2887×10^{-5}	39	$a = 1.402e \times 10^{-5}$ $b = 2.1416 \pm 0.1154$
Power-2 $f(x) = a x^b + c$	330	2.4641×10^{-8}	0.9968	0.9967	2.5464×10^{-5}	38	$a = 2.158 \times 10^{-5}$ $b = 2.0229 \pm 0.2849$ $c = -0.0002634$
Quadratic-1 $f(x) = p_1 x^2 + p_2 x + p_3$	300	9.0566×10^{-11}	0.9998	0.9998	1.5438×10^{-6}	38	$p_1 p_2 = 1.202 \times 10^{-5}$ $= -0.0001084$ $p_3 = 0.000336$
Quadratic-2 $f(x) = p_1 x^2 + p_2$	300	3.0223×10^{-9}	0.9927	0.9925	8.8031×10^{-6}	39	$p_1 p_2 = 5.271 \times 10^{-6}$ $= -8.994 \times 10^{-5}$
Power-1 $f(x) = a x^b$	300	2.5761×10^{-8}	0.9376	0.9360	2.5701×10^{-5}	39	$a = 3.64 \times 10^{-6}$ $b = 2.042 \pm 0.2323$
Power-2 $f(x) = a x^b + c$	300	2.9303×10^{-9}	0.9929	0.9925	8.7814×10^{-6}	38	$a = 4.918 \times 10^{-6}$ $b = 2.026 \pm 0.4274$ $c = -8.591 \times 10^{-5}$
Quadratic-1 $f(x) = p_1 x^2 + p_2 x + p_3$	270	$3.2430e \times 10^{-12}$	0.9995	0.9995	2.9213×10^{-7}	38	$p_1 p_2 = 1.766 \times 10^{-6}$ $p_2 = -1.721 \times 10^{-5}$ $= 5.463 \times 10^{-5}$
Quadratic-2 $f(x) = p_1 x^2 + p_2$	270	7.7208×10^{-11}	0.9893	0.9890	1.4070×10^{-6}	39	$p_1 p_2 = 6.949 \times 10^{-7}$ $= -1.303 \times 10^{-5}$
Power-1 $f(x) = a x^b$	270	1.6733×10^{-10}	0.9937	0.9937	1.3067×10^{-6}	98	$a = 1.489 \times 10^{-7}$ $b = 2.573 \pm 0.1149$
Power-2 $f(x) = a x^b + c$	270	8.0189×10^{-11}	0.9889	0.9883	1.4527×10^{-6}	38	$a = 6.94 \times 10^{-8}$ $b = 2.003 \pm 0.5312$ $c = -1.301 \times 10^{-5}$
Quadratic-1 $f(x) = p_1 x^2 + p_2 x + p_3$	240	1.8633×10^{-12}	0.9924	0.9918	2.8462×10^{-7}	97	$p_1 p_2 = 6.007 \times 10^{-7}$ $p_3 = -6.441 \times 10^{-6}$ $= 1.853 \times 10^{-5}$
Quadratic-2 $f(x) = p_1 x^2 + p_2$	240	2.7496×10^{-12}	0.9889	0.9889	3.3848×10^{-7}	23	$p_1 p_2 = 2.332 \times 10^{-7}$ $= -9.48 \times 10^{-6}$
Power-1 $f(x) = a x^b$	240	7.6145×10^{-12}	0.9944	0.9943	2.787×10^{-7}	98	1.252×10^{-9} $b = 4.0504 \pm 0.2125$
Power-2 $f(x) = a x^b + c$	240	2.9686×10^{-12}	0.9880	0.9869	3.5926×10^{-7}	23	$a = 2.321 \times 10^{-7}$ $b = 2.0041 \pm 1.2426$ $c = 3.79 \times 10^{-7}$
Quadratic-1 $f(x) = p_1 x^2 + p_2 x + p_3$	210	3.5188×10^{-13}	0.9930	0.9923	1.3982×10^{-7}	18	$p_1 p_2 = 5.242 \times 10^{-7}$ $p_3 = -6.897 \times 10^{-6}$ $= 2.384 \times 10^{-5}$
Quadratic-2 $f(x) = p_1 x^2 + p_2$	210	7.0210×10^{-13}	0.9861	0.9854	1.9223×10^{-7}	19	$p_1 p_2 = 1.443 \times 10^{-7}$ $= -7.321 \times 10^{-6}$
Power-1 $f(x) = a x^b$	210	4.2763×10^{-12}	0.9155	0.9111	4.7441×10^{-7}	19	$a = 7.981 \times 10^{-13}$ $b = 7.0066 \pm 0.8938$
Power-2 $f(x) = a x^b + c$	210	6.8143×10^{-13}	0.9865	0.9850	1.9457×10^{-7}	18	$a = 1.412 \times 10^{-7}$ $b = 2.0007 \pm 1.9340$ $c = 3.559e \times 10^{-8}$

Our investigation reveals that the field dependence studies of the sample is the non-ohmic nature i.e. the current exhibits an applied voltage dependence of the form $I \sim V^n$, where n is found to be greater than 1. On the other hand, it is known that, depending on the value of n , be three types of conduction mechanisms, namely SCLC, Schottky and Poole-Frenkel-type conduction may be relevant [24]. According to the SCLC theory the values of slope are 1 in the ohmic region and 2 in the square law region. The $\log I - \log V$ curves (Fig. 5) show a gradual transition from an ohmic region to the region where the current $\log I$ is proportional to $n (\log V)$ with $n = 2$. Therefore, we investigated various fits of the I-V

measurements for five different temperatures in the non-ohmic region. The details of these fits are given in Table 4. The columns of the table are: the fit type, SSE (Sum of squares due to error), r-squared (R-squared (coefficient of determination)), adj-squared (Degree of freedom adjusted coefficient of determination), RMSE (Root mean squared error (standard error)), dfe (Degrees of freedom in the error), fit parameters. These fits are given in Fig. 6. From these fit details we can conclude that all the fit models describes the data quite well, but the best fit is the $ax^b + c$, see Fig. 7.

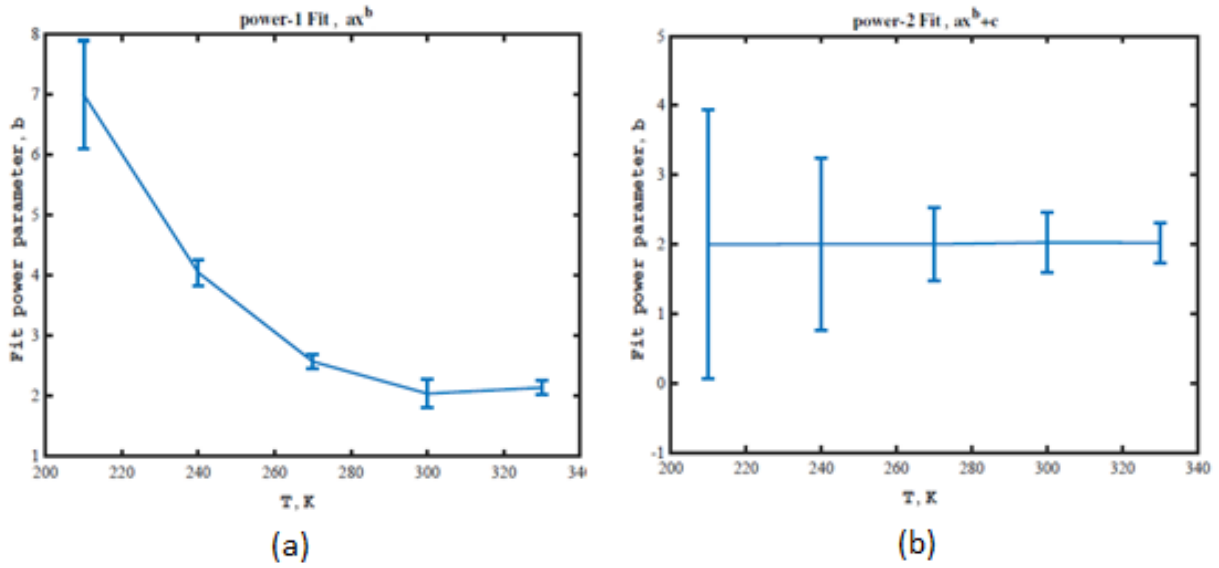


Fig. 7. Fit parameter b in power fits versus temperature (T)

We then conclude that the conduction mechanism cannot be either Schottky or Poole-Frenkel. Therefore, our measurements confirm that the SCLC mechanism dominates the electronic conduction in the nonlinear region. This mechanism is influenced by the traps. As the applied voltage is increased, a strong injection of the charge carrier in the sample takes place. For strong injection, the traps in the sample filled up and a space charge appears. As the applied voltage is increased further, very strong injection of charge carrier takes place, all the traps in sample will become filled and the square law behavior will appear. In the case of the SCLC process the detailed features of the non-linear I-V characteristics are revealed in the $\ln(I/V)$ versus V plot. Figure 10 shows the $\ln(I/V) - V$ characteristics at five different temperatures of the TlInSe₂ sample.

It is seen that the characteristic behavior in Fig. 9 is still of non-linear nature and the slopes of the curves are temperature dependent, as temperature increases the slopes decrease slightly. The temperature dependence of the current density J is given [40]

$$j = en_0\mu E \exp\left(\frac{V\varepsilon_0 K}{eN_t k_B T d^2}\right) \quad (2)$$

where E is the electric field, μ is mobility of the carriers, n_0 is concentration of the carriers, V is applied voltage, ε_0 is permittivity of free space, K is dielectric constant of the material, d is thickness of the material and N_t is the trap density. Equation (1) can be rewritten as

$$\frac{J}{V} = \frac{en_0\mu}{d} \exp\left(\frac{V\varepsilon_0 K}{eN_t k_B T d^2}\right) \quad (3)$$

thus, a plot of $\ln(I/V)$ versus V should yield a straight line

with slope $\left(\frac{\varepsilon_0 K}{eN_t k_B T d^2}\right)$ and intercept $\frac{en_0\mu}{d}$. Making

use of Eq. (1) and the intercepts of the $\ln(I/V)$ versus V plots in Fig. 9, trap densities for different temperatures were calculated. These values were shown in Table 5. We plotted this fit for the range of temperatures in Fig. 8.

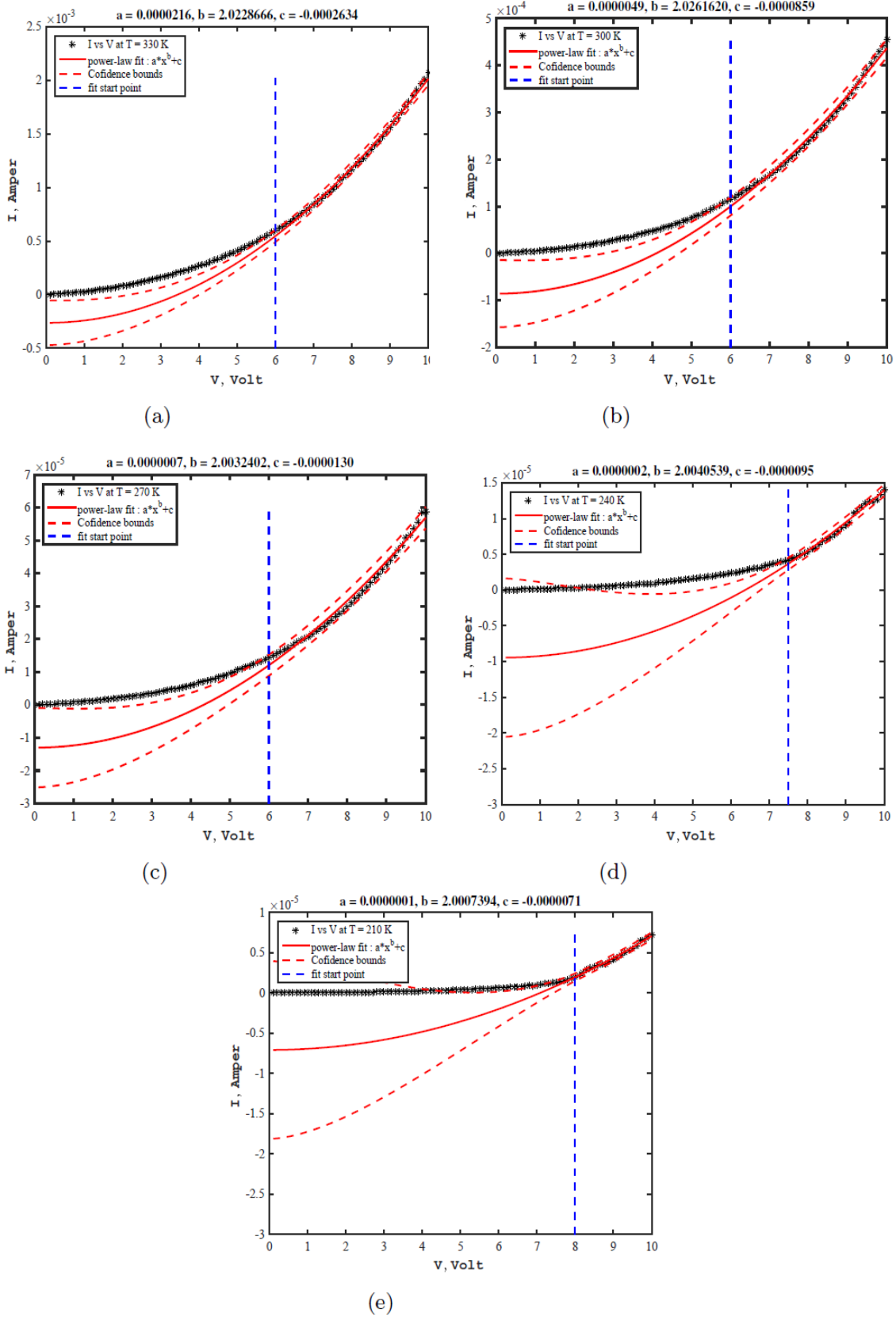


Fig. 8. Current (I) versus Voltage (V) data with $ax^b + c$ fit for the range of temperatures

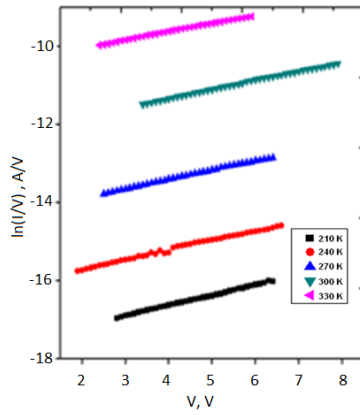


Fig. 9 $\ln(I/V)$ - V characteristics at different temperatures

Table 5. Variation of trap density with temperature

T(K)	$N_t(\text{m}^{-3} \text{eV})^{-1} \times 10^{18}$
210	1.04
240	0.95
270	0.88
300	0.83
330	0.82

It is further seen that the values for $n_0\mu$ can be calculated by using the intercepts in Eq. (2). The mobility of carriers exhibits a trap activated temperature relation of the form [34].

$$n_0\mu = n_0\mu_0 \exp\left(-\frac{E_t}{k_B T}\right) \quad (4)$$

where E_t is the activation energy of the traps. It is possible to extract information about the activation energy of the traps by plotting $\ln n_0\mu$ versus $1/T$ (Fig. 10). It is seen that the plot is linear and the value of E_t is calculated to be 26 meV. This value is in close agreement with those reported in Ref. [15].

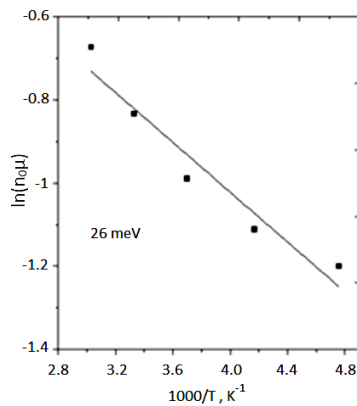


Fig. 10. $\ln(n_0\mu)$ - $10^3/T$ characteristics of TlInSe₂.

3.4. AC Conductivity

The ac conductivity (σ_{ac}) was studied over a

frequency range of 10 Hz to 20 MHz, for temperature varying from 173 to 373 K. The frequency dependence of the ac conductivity σ_{ac} of TlInSe₂ crystal over the temperature range is shown in Fig. 11.

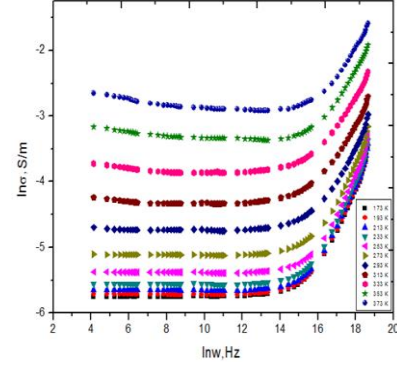


Fig. 11. Frequency dependence of ac conductivity for TlInSe₂ ternary compound at different temperature

The obtained curves consist of two regions; at low frequencies, an almost frequency independent region. Here, we conclude that dominant mechanism is dc conductivity. At high frequencies, the conductivity increases gradually with increasing frequency. The dependence of ac conductivity on frequency can be expressed by the following equation [41]

$$\sigma_{ac}(\omega) = \sigma_{tot} - \sigma_{dc} = A\omega^s \quad (5)$$

Where ω is the angular frequency, σ_{tot} is the total electrical conductivity, σ_{dc} is the dc electrical conductivity, A is constant dependent on temperature and s is the frequency exponent. This exponent is used to characterize the electrical conduction mechanism in different materials. Values of the frequency exponent s were obtained from the slopes of the straight lines in Fig.11 for high ranges of frequencies. The temperature dependent parameters s for the investigated sample is shown in Fig. 12.

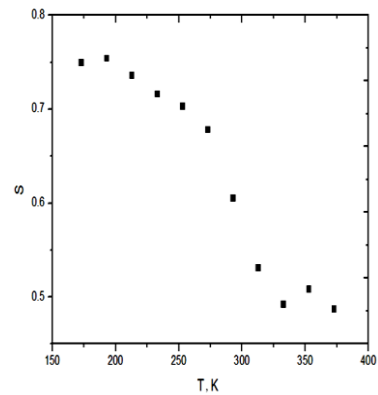


Fig. 12. Temperature dependence of the frequency exponent s for TlInSe₂ ternary compound.

It is seen that the frequency exponent s decreases with increasing temperature. To determine the predominant conduction mechanism under ac field for the studied sample, different theoretical models have been proposed.

In the quantum mechanical tunneling (QMT) model [42], the exponent s is almost equal to 0.8 and increases slightly with temperature or independent of temperature. In the overlapping-large polaron tunneling (QLPT) model [42], the exponent s is both frequency and temperature dependent and decreases with increasing temperature to a minimum value at a certain temperature, then it increases with increasing temperature. Therefore, the QLPT and QMT models are not applicable to the obtained results. It is clear in Fig. 12 that the value of s decreases with the increase in temperature. The decreases of s with increasing temperature are similar to those observed in chalcogenide glasses, amorphous and crystalline semiconductors [43]. Therefore, the Correlated Barrier Hopping model is applicable to this sample [41-44]. In this model thermally activated hopping of the charge carriers over the energy barrier separating two localized sites is assumed [45]. The frequency exponent s for this model is given by

$$s = 1 - \frac{6k_B T}{W_m} \quad (6)$$

where k_B is the Boltzmann constant, T is the absolute temperature and W_m , is the maximum barrier height which is called binding energy. W_m the binding energy is described as the energy required to move an electron from one site to another site [44]. Using the above calculated value of s , the maximum barrier height was calculated according to Eq. 4 and is found to be 0.38 e V for the room temperature.

The temperature dependence of σ_{ac} at different frequencies is shown in Fig. 13.

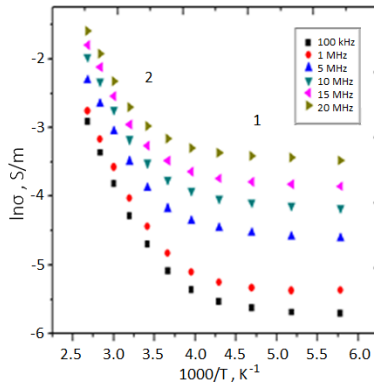


Fig. 13. Temperature dependence of ac conductivity for TIInSe₂ ternary compound at different frequencies

This figure shows that there are two straight lines in each plot with different slopes which suggests two different regions with different activation energies, one with weak temperature dependence and the other with strong temperature dependence. These regions obey the Arrhenius equation:

$$\sigma = \sigma_0 \exp(-E/k_B T) \quad (7)$$

where σ_0 is the pre-exponential factor, k_B is the Boltzmann constant, T is the absolute temperature and E is the conduction activation energy. The values of the activation energy E_1 and E_2 for both regions were calculated from the slope of $\ln \sigma$ versus $10^3/T$ curves and

are given Table 6.

Table 6. Activation energy values

Frequency (MHz)	Activation energy (eV)	
	E1	E2
0.1	0.023	0.19
1	0.020	0.18
5	0.016	0.17
10	0.016	0.16
15	0.014	0.15
20	0.011	0.14

As shown in Table 6, the activation energy, E decreases with the increasing frequency. In the first region ($T \leq 253$ K), the obtained low values of activation energy suggests that the conduction mechanism may be due to the hopping of electrons [42-45]. In the second region ($T \geq 253$ K), the values of activation energy indicates that the conductivity is a thermally activated process. It can be analyzed according to the Eq. 7.

4. Conclusion

The characteristic vibrational frequencies of TIInSe₂ crystal were observed using Micro Raman spectrometer and the obtained frequencies are in good agreement with previously reported Raman results for TIInSe₂. In addition the assignment of the TIInSe₂ Raman bands was supported on a normal mode calculation for the TIIn₄Se₁₆ cluster, as a model.

The electrical properties of TIInSe₂ sample have been investigated in the temperature range 120-330 K. The electrical conductivity increases with increasing temperature for these samples. The dependence of ohmic resistance on temperature is the one corresponding to thermally activated processes. The activation energy for electrical conduction has a value of about 0.34 eV, which is usual for this type of chalcogenide semiconductors. The present study shows that the variation of current with voltages for the sample follows Ohm's law at low voltages but deviates from Ohm's law at high voltages. According to the experimental evidence presented, non-linear behavior may be attributed in principle to an SCLC type conduction mechanism. The activation energy of the traps is estimated as 26 meV. The trap density is found to decrease for increasing temperature.

Ac conductivity was found to obey the power law ω^s , where $s < 1$ and σ_{ac} increases with increasing frequency. The frequency exponent s was found to be decrease with increasing temperature which indicates that the correlated barrier hopping is the most probable mechanism. The smaller activation energy values confirm that the CBH model is the most dominant mechanism contributing to the ac conduction in the investigated samples.

Acknowledgements

The authors would like to thank Assist. Prof. Dr. N. Akcay, University of Istanbul, Nanotechnology Research Laboratory, for performing some of the electrical

measurements, Assoc. Prof. Dr. A. Kizilersu and Prof. Dr. D. Deger for many helpful suggestions and critical reading of the manuscript.

References

- [1] A. M. Badr, I. M. Ashraf, *Phys. Scr.* **86**, 035704 (2012).
- [2] N. M. Gasanly, T. Yildirim, *Acta Phys. Pol.* **119**, 437 (2011).
- [3] A. F. Qasrawi, N. M. Gasanly, *Mater. Res. Bull.* **46**, 1227 (2011).
- [4] S. Hosokawa, K. Kamimura, H. Ikemato, et al. *Phys. Status Solidi B* **252**, 1225 (2015).
- [5] O. Z. Alekperov, M. A. Aljanov, E. M. A. Kerimova, *J. Phys.* **22**, 1053 (1998).
- [6] B. Abay, B. Gurbulak, M. Yildirim, H. Efeoglu, Y. K. Yogurtcu, *Phys. Status Solidi A* **153**, 145 (1996).
- [7] Ch. Karkotsou, M. Hantias, A. N. Anagnostopoulos, K. Kambas, G. Bleris, *Cryst. Res. Technol.* **31**, 41 (1996).
- [8] H. A. Elshaikh, *Cryst. Res. Technol.* **31**, 903 (1996).
- [9] Ch. Karkotsou, A. N. Anagnostopoulos, *Physica D* **93**, 157 (1996).
- [10] M. Hantias, A. N. Anagnostopoulos, K. Kambas, J. Spyridelis, *Phys. Rev. B* **43**, 4134 (1991).
- [11] D. G. Kilday, D. W. Niles, G. Margaritondo, *Phys. Rev. B* **35**, 660 (1987).
- [12] A. E. Bakhyshev, M. F. Agaeva, A. M. Darvish, *Phys. Status Solidi B* **91**, K 31 (1979).
- [13] R. S. Madatov, A. I. Najafov, Yu. M. Mustafayev et al., *Semicond.* **49**, 1166 (2015).
- [14] A. A. Ebnalwaled, R. H. Al-Orainy, *Appl. Phys. A* **112**, 955 (2013).
- [15] A. F. Qasrawi, N. M. Gasanly, *Phys. Status Solidi A* **208**, 1688 (2011).
- [16] A. Kh. Matiyev, A. N. Georgobiani V. V. Kodin, M. A. Matiyev, *Ferroelectrics* **397**, 198 (2010).
- [17] J. Grigas, E. Talik, M. Adamiec, V. Lazauskas, V. Nelkinas, *Lithuanian J. Phys.* **47**, 87 (2007).
- [18] I. V. Alekseev, *Inorg. Mater.* **41**, 796 (2005).
- [19] G. L. Myronchuk, O. V. Zamurueva, K. Ozga et al., *Archives Metallurgy and Mater.* **60**, 1051 (2015).
- [20] R. R. Rosul, P. P. Guranich, O. O. Gomonnai et al., *Semicond. Phys., Quantum Elect. & Optoelect.* **15**, 35 (2012).
- [21] S. E. Al Garni, *Life Sci. J* **8**, 560 (2011).
- [22] N. M. Gasanly, *J. Korean Phys. Soc.* **48**, 914 (2006).
- [23] A. N. Georgobiani, A. Kh. Matiev, B. M. Khamkhoev, A. M. Evloev, *Inorg. Mater.* **41**, 224 (2005).
- [24] N. Kalkan, H. Bas, *J. Elect. Mater.* **44**, 4387 (2015).
- [25] N. Kalkan, S. Yildirim, K. Ulutas, D. Deger, *J. Electron Mater.* **37**, 157 (2008).
- [26] N. Kalkan, S. Yildirim, D. Deger, K. Ulutas, Y. Gurkan Celebi, *Mater. Res. Bull.* **40**, 936 (2005).
- [27] K. Ulutas, N. Kalkan, S. Yildirim, D. Deger, *Cryst. Res. and Technol.* **40**, 898 (2005).
- [28] A. I. Mukolu, *Turk J. Phys.* **25**, 385 (2001).
- [29] Von D. Muller, G. Eulenberger, H. Harn, *Z. Anorg. Allg. Chem.* **398**, 207 (1973).
- [30] N. M. Gasanly, A. F. Goncharov, B. M. Dzhavadov et al., *Phys. Status Solidi (b)* **92**, K139 (1979).
- [31] N. M. Gasanly, B. M. Dzhavadov, V. I. Tagirov et al., *Phys. Status Solidi B Basic Research* **97**, 367(1980).
- [32] M. J. Frisch, G. W. Trucks, H. B. Schlegel, G. E. Scuseria, M. A. Robb, J. R. Cheeseman, V. G. Zakrzewski, J. A. Montgomery, R. E. Stratmann, J. C. Burant, S. Dapprich, J. M. Millam, A. D. Daniels, K. N. Kudin, M. C. Strain, O. Farkas, J. Tomasi, V. Barone, M. Cossi, R. Cammi, B. Mennucci, C. Pomelli, C. Adamo, S. Clifford, J. Ochterski, G. A. Petersson, P. Y. Ayala, Q. Cui, K. Morokuma, D. K. Malick, A. D. Rabuck, K. Raghavachari, J. B. Foresman, J. Cioslowski, J. V. Ortiz, A. G. Baboul, B. B. Stefanov, G. Liu, A. Liashenko, P. Piskorz, I. Komaromi, R. Gomperts, R. L. Martin, D. J. Fox, T. Keith, M. A. Al-Laham, C. Y. Peng, A. Nanayakkara, M. Challacombe, P. M. W. Gill, B. Johnson, W. Chen, M. W. Wong, J. L. Andres, C. Gonzalez, M. Head-Gordon, E. S. Replogle, J. A. Pople, *Gaussian 03, (Revision B.04)* (Inc. Pittsburgh, PA, 2003).
- [33] T. Sundius, *J. Molecular Structure* **218**, 321 (1990). (T. Sundius, MOLVIB 7.0 QCPE Program No. 807, 2002).
- [34] T. Sundius, *Vib. Spectrosc.* **29**, 89 (2002).
- [35] M. D. Ward, E. A. Pozzi, R. P. Van Duyne, J. A. Ibers, *J. Solid State Chem.* **212**, 191 (2014).
- [36] Douglas Bodie, Ho Shi-Ming, *Structure and Chemistry of Crystalline Solids* (Springer Verlag, New York, 2006) p. 162.
- [37] K. Stelmaszczyk, C. Schultz, M. Schuele, M. Weizman, C. A. Kaufmann, R. Schlatmann, B. Rau, V. Quaschnig, B. Stegemann, F. Fink, *Thin-Film CIGS Degradation under P2 Scribe Laser Illumination, Investigation of 29th European Photovoltaic Solar Energy Conference and Exhibition, 3DV.1.55* (2014) p.1763.
- [38] *Non-Tetrahedrally Bonded Elements and Binary Compounds I, Vol. 41C of the series Landolt-Börnstein D Group III Condensed Matter* (1998) p.1.
- [39] D. M. Adams, E. A. V. Ebsworth, *Spectroscopic Properties of Inorganic and Organometallic Compounds* (Royal Society of Chemistry, London 1981) p.184.
- [40] M. A. Lampert, P. Mark, *Current injections in solids* (NY Lond. 1970).
- [41] M. Ganaie, M. Zulfeqar, *Acta Phys. Pol.* **128**, 59 (2015).
- [42] D. Deger, K. Ulutas, S. Yakut, *J. Ovonic Res.* **8**, 179 (2012).
- [43] H. M. El-Mallah, *Acta Phys. Pol.* **122**, 174 (2012).
- [44] D. Deger, K. Ulutas, S. Yakut, H. Kara, *Mater. Sci. in Semicond. Processing* **38**, 1 (2015).
- [45] Y. Ben Taher, A. Oueslati, N. K. Maaloul, K. Khirouni, M. Gargouri, *Appl. Phys. A* **120**, 1537 (2015).
- [46] M. Okutan, E. Basaran, H. I. Bakan, F. Yakuphanoglu, *Phys. B* **364**, 300 (2005).

*Corresponding author: nkalkan@istanbul.edu.tr